XLIII CILAMCE
21–25, November, 2022
FOZ DO IGUAÇU – PR – BRAZIL

Study of Ballistic Parameters for Projectile Range Extension

Wallace Ramos Rosendo da Silva[1], André Luiz Tenório Rezende[1]

[1]*Dept. of Mechanical and Materials Engineering, Brazilian's Army Military Institute of Engineering*
Praça General Tibúrcio, 80 - Praia Vermelha, 22290-270, Rio de Janeiro/RJ, Brazil
wrosendoeng@ime.eb.br, arezende@ime.eb.br

Abstract. The external ballistics of an artillery shell requires an understanding of aerodynamics in compressible flow. In this context, computational fluid dynamics (CFD) techniques are used because real tests with ammunitions are more expensive than numerical simulations. The purpose of this study is to simulate the use of downstream hot mass flow injection, which is technically called base bleed, because it increases base pressure to an optimal value that reduces base drag, which is the main component of the total aerodynamic drag. The compressible, stationary and two-dimensional axisymmetric flow around the projectile is simulated and analyzed. For the simulations, the SST k-ω turbulence model is used, based on the Reynolds means (RANS). The results are compared with a specific commercial program for application in weapons ballistics. The main results are the velocity, pressure and temperature fields; in addition to obtaining drag coefficients for different situations of boundary conditions.

Keywords: External ballistics, aerodynamics, range extension

1 Introduction

Projectile range extension is a matter of great interest in aerodynamics field. The complexity presented due to influence of compressibility and high Reynolds number, then a lot of techniques could be used to understand how forces acting over the ammunition. Firing test is a good example for obtaining real values of interesting properties, however it is expensive and requires many people for reproducing. The same applies for wind-tunnel tests, with addition of creating similarity condition of flight. Thus, computational fluid dynamics (CFD) shows itself as a cheaper method with reasonable results.

In this paper, the drag force will be discussed because it is the main responsible for air resistance during flight [1]. There are two principal ways to produce drag: viscous (skin friction drag) and pressure (surface and base drag). Base drag represents the main portion of total drag at supersonic speeds, around 50% [2], then reducing it with hot gas injection, increasing base pressure at an optimal value. This method is commonly used in a technology named *base bleed* (BB) and ammunitions that use it are referred as "extended range" munition (ER).

2 Mathematical Modelling

2.1 Compressible Governing Equations

In this present work, Navier-Stokes equations are solved as a prerequisite of finite-volume method for describing conservation of mass (1), momentum (2) and energy (3):

$$\frac{\partial \rho}{\partial t} + \nabla \cdot (\rho \mathbf{v}) = 0 \tag{1}$$

$$\frac{\partial}{\partial t}(\rho \mathbf{v}) + \nabla \cdot \{\rho \mathbf{v}\mathbf{v}\} = \nabla \cdot \{\mu \nabla \mathbf{v}\} - \nabla p + \nabla \cdot \left\{\mu \left(\nabla \mathbf{v}\right)^T\right\} - \frac{2}{3}\nabla \left(\mu \nabla \cdot \mathbf{v}\right) \tag{2}$$

$$\frac{\partial (\rho T)}{\partial t} + \nabla \cdot (\rho T \mathbf{v}) = \nabla \cdot \left(\frac{\mu}{Pr} \nabla T\right) \tag{3}$$

Where ρ is the density, $\mathbf{v}$ is the vector form of velocity, p denotes pressure, T is the local temperature. Pr is the Prandtl number ($Pr = \frac{c_p \mu}{k}$), c_p and k are heat capacity at constant pressure and the thermal conductivity, respectively. Considering air as an ideal gas, the viscosity could be modelled as Sutherland's law (4):

$$\mu = \frac{C_1 T^{3/2}}{T + S} \tag{4}$$

C_1 and S are equal to 1.458 $\times 10^{-6}$ $\mathrm{kg\,m^{-1}\,s^{-1}\,K^{-1/2}}$ and 110.4 K, respectively. As a consequence of ideal gas law, pressure is defined by $p = \rho RT$, with R described as specific gas constant (287.05 $\mathrm{J\,kg^{-1}\,K^{-1}}$).

2.2 Boussinesq Hypothesis

The Reynolds-Averaged Navier-Stokes models depend on the definition of the Reynolds stress tensor ($\boldsymbol{\tau}^R$), which is a linear function of the mean velocity gradients such that:

$$\boldsymbol{\tau}^R = -\rho\overline{\mathbf{v}'\mathbf{v}'} = \mu_t \left\{ \nabla\mathbf{v} + (\nabla\mathbf{v})^T \right\} - \frac{2}{3}\left[\rho k + \mu_t \left(\nabla \cdot \mathbf{v}\right)\right]\mathbf{I} \tag{5}$$

where k is the turbulent kinetic energy ($k = \frac{1}{2}\overline{\mathbf{v}' \cdot \mathbf{v}'}$), the superscript T is the transpose matrix and $\boldsymbol{I}$ is the identity matrix.

2.3 Shear Stress Transport k-w model

The Shear-Stress Transport (SST) k-ω model of Menter [3] is based on two-equations to describe eddy viscosity (6), which is proposed such that

$$\mu_t = \frac{\rho a_1 k}{\max(a_1\omega; \sqrt{2}S_t F_2)} \tag{6}$$

where a_1 = 0,31, S_t is the magnitude of the strain rate ($S_t = \sqrt{\boldsymbol{S}_t \cdot \boldsymbol{S}_t}$) and F_2 is given by

$$F_2 = \tanh\left(\max\left(2\frac{\sqrt{k}}{0.09\omega y}; \frac{500\nu}{y^2\omega}\right)^2\right) \tag{7}$$

the y denotes the shortest distance from wall. The transport equations of scalars k and ω are defined in (8) and (9):

$$\frac{\partial}{\partial t}(\rho k) + \nabla \cdot (\rho\mathbf{v}k) = \nabla \cdot \left[\left(\mu + \sigma_k\mu_t\right)\nabla k\right] + \tilde{P}_k - \beta^*\rho k\omega \tag{8}$$

$$\frac{\partial}{\partial t}(\rho\omega) + \nabla \cdot (\rho\mathbf{v}\omega) = \nabla \cdot \left[\left(\mu + \sigma_\omega\mu_t\right)\nabla\omega\right] + \alpha\frac{1}{\nu_t}\tilde{P}_k - \beta\rho\omega^2 + 2(1 - F_1)\sigma_{\omega 2}\frac{\rho}{\omega}\nabla k \cdot \nabla\omega \tag{9}$$

The $\tilde{P}_k$ represents production of turbulence kinetic energy and is demonstrated as by (**??**):

$$\tilde{P}_k = \min\left(\mu_t\nabla\mathbf{v} \cdot \left(\nabla\mathbf{v} + (\nabla\mathbf{v})^T\right); 10 \cdot \beta^*\rho k\omega\right) \tag{10}$$

and the blending function F_1 is related to the wall distance and is given as

$$\alpha = \alpha_1 F_1 + \alpha_2(1 - F_1) \tag{11}$$

$$F_1 = \tanh\left(\min\left[\max\left(\frac{\sqrt{k}}{0.09\omega y}; \frac{500\nu}{y^2\omega}\right); \frac{4\rho\sigma_{\omega 2}k}{CD_{k\omega}y^2}\right]^4\right) \tag{12}$$

$$CD_{k\omega} = \max\left(2\rho\sigma_{\omega 2}\frac{1}{\omega}\nabla k \cdot \nabla\omega; 10^{-10}\right) \tag{13}$$

The constants for this model are defined by [3, 4]: $\beta^* = 0.09$; $\alpha_1 = 5/9$; $\beta_1 = 3/40$; $\sigma_{k1} = 0.85$; $\sigma_{\omega 1} = 0.5$; $\alpha = 0.44$; $\beta_2 = 0.0828$; $\sigma_{k2} = 1.0$; $\sigma_{\omega 2} = 0.856$.

3 Numerical Methods

The solver used in this paper is based on finite-volume method (FVM). The algorithm solves governing equations simultaneously and after that, turbulence equations are calculated. This technique demands many iterations

until convergence. The simulations considered a two-dimensional axissymetric mesh because of projectile geometry. Second-order upwind scheme is applied for spatial discretization. Convergence criteria is 1.0 x 10^{-6} for all properties of interest. Multigrid method, created by Hutchinson and Raithby [5], is used for algebraic resolution of partial-differential equations.

3.1 Mesh and Boundary Conditions

The ammunition analyzed in this article is 155mm M107 with simplifications in geometry to avoid numerical errors. Two meshes were developed in ANSYS Meshing 2021R2® for validation of CFD application with boundary conditions such as explained in Fig. 1. Initially, for pre-processing simulations an initial mesh with approximately 187.000 elements was developed, and then, a refined mesh with 380.000 elements. In both regions the domain size is 21L x 20D, being L and D the projectile reference length and diameter, respectively.

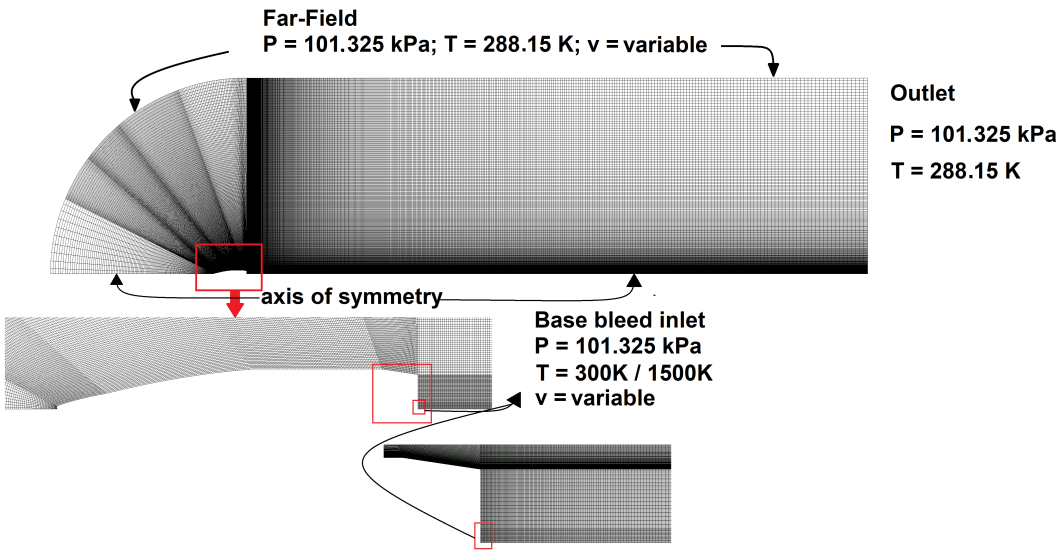

Figure 1. Mesh discretization and boundary conditions

Due to thermodynamic relations, this flow is considered isentropic. Therefore, the velocities of free stream and base-bleed system are prescribed as a function of Mach number (Ma) and boundary condition temperatures, $\mathrm{v} = \mathrm{Ma}\sqrt{\gamma \mathrm{RT}}$.

4 Results

4.1 Evalution Parameters

The first parameter of mesh analysis used in this paper is the drag coefficient. This non-dimensional coefficient describe how the drag force, the main air resistance during flight, acts in the profile of interest. Its equation is given by eq. (14)

$$C_D = \frac{F}{\frac{1}{2}\rho_\infty \mathrm{v}_\infty^2 A_{ref}} \tag{14}$$

where F is the axial force, $\frac{1}{2}\rho_\infty \mathrm{v}_\infty^2$ denotes the dynamic pressure, with ρ_∞ and v_∞ being the density and velocity in the free air stream and A_{ref} is the projectile reference area. About that, there is a dimensionless variable named injection parameter I that Belaidouni et al. [6] defines it as the bleed mass flow rate $\dot{m}$ normalized by the product of the free stream mass flux passing by base surface area A_{base}, described as eq. (15).

$$I = \frac{\dot{m}}{\rho_\infty \mathrm{v}_\infty A_{base}} \tag{15}$$

4.2 CFD without Base Bleed

The Figure 2 shows a first validation without base bleed to compare similar calculations among the results and a reference developed by Mahmoud et al. [7]. The Figure 3a shows that the refined mesh (380K) elements demonstrated better agreement than the initial mesh in transonic and supersonic regimes, which represent most part of projectile firing.

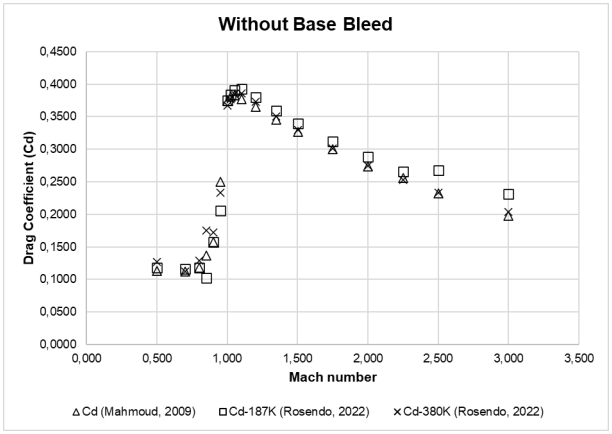

Figure 2. Drag coefficient without base bleed

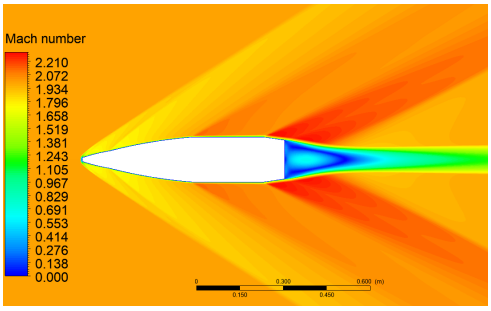

(a) Base bleed off

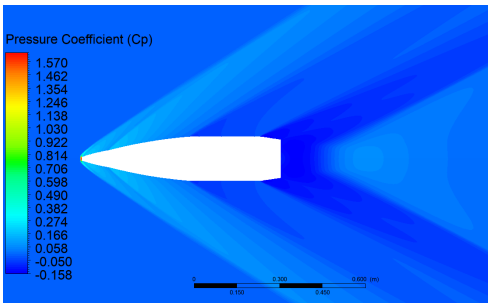

(b) Base bleed off

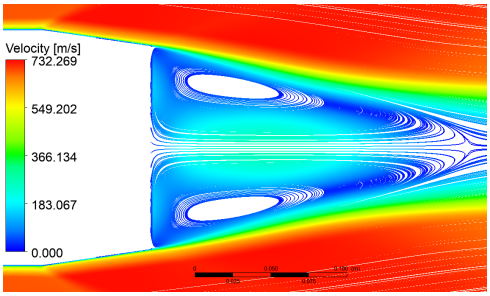

(c) Base bleed off

Figure 3. Contours of Velocity and Pressure and Streamline Velocities with Ma = 2.0

The contours of velocity in Fig. 3a and pressure in Fig. 3b are determined by non-dimensional parameters Mach number and pressure coefficient, respectively. These contours were obtained with Ma $=$ 2.0 at far-field boundary condition. The Figure 3c demonstrates the recirculation zone caused by the lowest values of pressure and, consequently, velocity. About the pressure coefficient, it is a relation between static and dynamic pressure, represented in (16):

$$C_P \equiv \frac{\mathrm{p} - \mathrm{p}_\infty}{\frac{1}{2}\rho_\infty \mathrm{v}_\infty^2} \tag{16}$$

4.3 CFD with Base Bleed

After first validation, the base bleed technology was implemented in CFD analysis (see Fig. 4). Lucena et al. [1] explains that temperature has small influence in reducing drag and the results confirmed that statement, even though the values for base bleed injecting gases in 1500K showed lower values than inert projectile (base bleed off) or than cold injection (base bleed at T = 300K) in supersonic regimes.

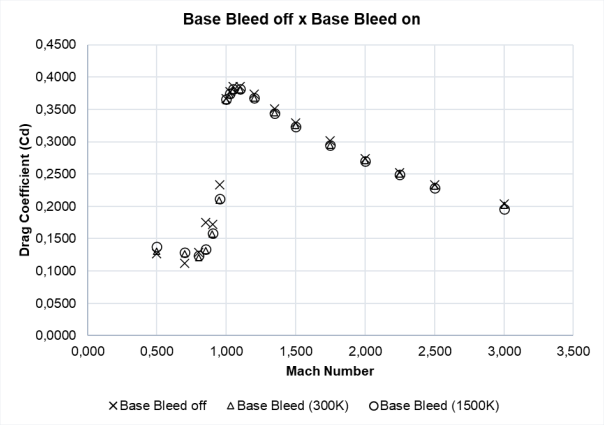

Figure 4. Drag coefficient without base bleed, comparing with Mahmoud et al. [7].

The Figures 5a and 5b display the contours of velocity assuming Mach number equals 2.0 at free air stream. At temperature T = 1500K, the base bleed creates a new recirculation zone, illustrated in Fig. 5b and Fig. 5f and gases were injected at Ma $\equiv$ 0.5. Despite the fact, the velocity contours at T = 300K in Fig. 5a does not alter significantly projectile in the downstream, which is noticed in streamlines of Fig. 5e. Besides that, in both cases, the base pressure was not increase sufficiently, as exhibited in Fig. 5c and Fig. 5d.

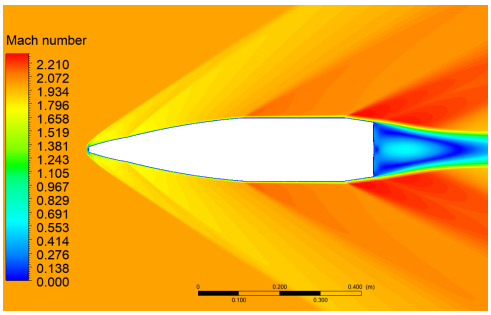

(a) $T_{BB} = 300K$

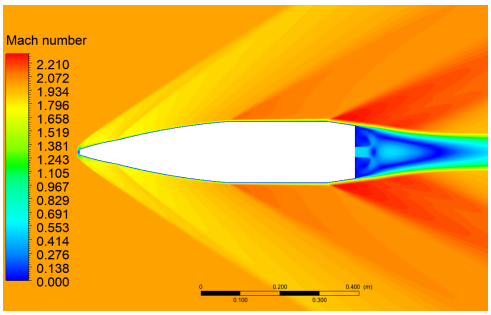

(b) $T_{BB} = 1500K$

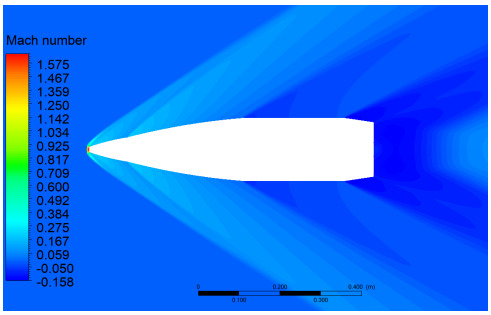

(c) $T_{BB} = 300K$

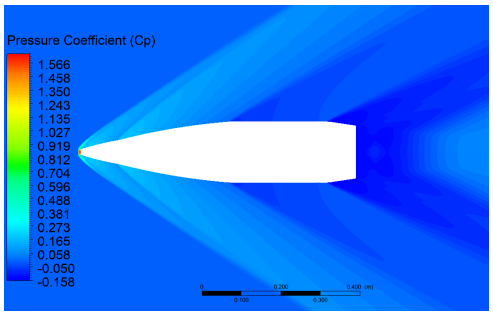

(d) $T_{BB} = 1500K$

Figure 5. Contours of Velocity and Pressure and Velocity streamlines with Ma = 2.0

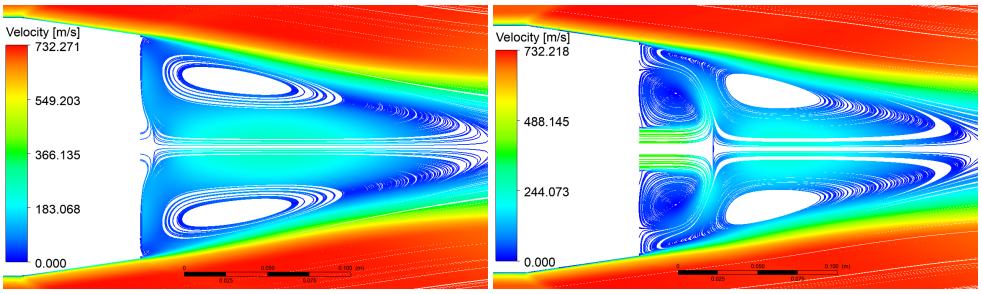

(e) $T_{BB} = 300K$ (f) $T_{BB} = 1500K$

Figure 5. Contours of Velocity and Pressure and Velocity streamlines with Ma = 2.0

4.4 Ballistic Performance

The influence of CFD analysis undergoes trajectory modelling. Thus, because of geometry and stabilization method, the projectile trajectory could be modelled with the modified point-mass trajectory model (MPMTM) proposed by Lieske and Reiter [8]. Actually, this four degrees-of-freedom (4-DOF) model is used to standardize the exterior ballistic trajectory simulation methodology for North Atlantic Treaty Organization (NATO), as explained in [9]. It is also elucidated that demands less requirements to flight prediction if compared to six degrees-of-freedom (6-DOF) model with reasonable results.

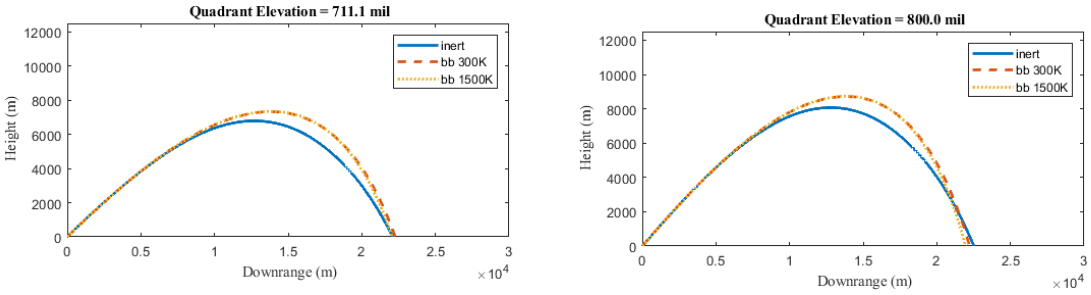

(a) 711 mil (40 degrees) (b) 800 mil (45 degrees)

Figure 6. Trajectories in different Quadrant Elevations, comparing inert and active base bleed.

The Figure 6 exhibits the results of a code designed in MATLAB® to prove its efficiency, comparing flight paths of projectile without base bleed (inert), with base bleed at T = 300K (cold injection) and base bleed at T = 1500K (hot injection) at different quadrant elevations (QE). The downrange and apogee for every base bleed condition is described in Tab. 1. In both QE conditions, the apogee increased around 8% with base bleed injection, however its system does not influenced in downrange improvement.

Table 1. Results of flight prediction with Modified Point-Mass Trajectory Model

Quadrant Elevation	Downrange (Inert)	Downrange (BB)	Increment (%)	Apogee (Inert)	Apogee (BB)	Increment (%)
711 mil (bb T = 300K)	22097.4	22270.7	0.8	6971.4	7328.2	7.9
711 mil (bb T = 1500K)	22097.4	22056.6	-0.2	6971.4	7347.1	8.2
800 mil (bb T = 300K)	22514.4	22225.1	-1.3	8067.3	8713.5	8.0
800 mil (bb T = 1500K)	22514.4	21949.2	-2.5	8067.3	8735.3	8.3

5 Conclusions

In this paper, the application of base bleed system was suggested due to understand how drag force could be reduced with increment of base pressure. The SST k-ω model was a good choice for modelling turbulence in inert projectile drag coefficient, what was expected due to validation of this turbulence resource for aerodynamic issues. Both meshes agreed with reference values, especially the refined one.

Thereupon, the influence of temperature of gases was tested to evaluate if this property infers, but what was found is just a slight reduction of base drag. It did not help to discover what occurs with accuracy during injection of hot gases in downstream. Figures 5c and 5d confirmed that base pressure was not increased sufficiently.

In this study the velocity and temperature have been imposed to find mass flow rate for base bleed inlet boundary condition, however this imposition was not enough to predict drag coefficient, in agreement Dali and Jaramaz [10] and Lucena et al. [1]. Therefore, in future works it is expected that Base Bleed could be studied in different assumptions in geometry and formulations in internal ballistics issues.

Acknowledgements. The authors gratefully acknowledge the support from the Brazilian research agencies CAPES (Coordenação de Aperfeiçoamento de Pessoal de Nível Superior), FAPERJ (Fundação de Apoio à Pesquisa do Estado do Rio de Janeiro), and CNPq (Conselho Nacional de Desenvolvimento Científico e Tecnológico).

Authorship statement. The authors hereby confirm that they are the sole liable persons responsible for the authorship of this work, and that all material that has been herein included as part of the present paper is either the property (and authorship) of the authors, or has the permission of the owners to be included here.

References

[1] R. Lucena, N. Mangiavacchi, J. Pontes, G. Pinheiro, W. Rosendo, L. Neubarth, M. Ferrapontoff Lemos, and L. Júnior. Numerical aerodynamic simulation of an artillery projectile with a base bleed system, 2020.
[2] J. Sahu and K. R. Heavey. Numerical investigation of supersonic base flow with base bleed. *Journal of Spacecraft and Rockets*, vol. 34, n. 1, pp. 62–69, 1997.
[3] F. R. Menter. Two-equation eddy-viscosity turbulence models for engineering applications. *AIAA Journal*, vol. 32, pp. 1598–1605, 1994.
[4] F. R. Menter. Review of the shear-stress transport turbulence model experience from an industrial perspective. *International Journal of Computational Fluid Dynamics*, vol. 23, n. 4, pp. 305–316, 2009.
[5] B. R. Hutchinson and G. D. Raithby. A multigrid method based on the additive correction strategy. *Numerical Heat Transfer*, vol. 9, n. 5, pp. 511–537, 1986.
[6] H. Belaidouni, S. Zivkovic, and M. Samardzic. Numerical simulations in obtaining drag reduction for projectile with base bleed. *Scientific Technical Review*, vol. 66, pp. 36–42, 2016.
[7] O. Mahmoud, M. A. Suliman, M. Al-Sanabawy, and O. Abdel-Hamid. Computational investigation of base drag reduction for a projectile at different flight regimes, 2009.
[8] R. Lieske and M. Reiter. Equations of motion for a modified point mass trajectory. *Ballistic Research Laboratories*, vol. 1, n. 1, pp. 24, 1966.
[9] *The Modified Point Mass and Five Degrees of Freedom Trajectory Models - STANAG 4355*. NATO, 2009.
[10] M. A. Dali and S. Jaramaz. Optimization of artillery projectiles base drag reduction using hot base flow. *Thermal Science*, vol. 2018, pp. 210–210, 2018.